# Tuning pore dimensions of mesoporous inorganic films by homopolymer swelling

Barry Reid,[†] Alberto Alvarez-Fernandez,[†] Benjamin Schmidt-Hansberg,[‡] and Stefan Guldin[*,†]

[†]*Department of Chemical Engineering, University College London, Torrington Place, London, WC1E 7JE, UK*

[‡]*BASF SE, Process Research & Chemical Engineering, Coating & Film Processing, Carl-Bosch-Strasse 38, 67056 Ludwigshafen am Rhein, Germany*

E-mail: s.guldin@ucl.ac.uk

**Abstract**

The functionality and applications of mesoporous inorganic films are closely linked to their mesopore dimensions. For material architectures derived from block copolymer (BCP) micelle co-assembly, the pore size is typically manipulated by changing the molecular weight corresponding to the pore-forming block. However, bespoke BCP synthesis is often a costly and time-consuming process. An alternative method for pore size tuning involves the use of swelling agents, such as homopolymers (HPs), which selectively interact with the core-forming block to increase the micelle size in solution. In this work, poly(isobutylene)-*block*-poly(ethylene oxide) (PIB-*b*-PEO) micelles were swollen with poly(isobutylene) HP in solution and co-assembled with aluminosilicate sol with the aim of increasing the resulting pore dimensions. An analytical approach implementing spectroscopic ellipsometry (SE) and ellipsometric porosimetry (EP) alongside the more commonly used atomic force microscopy (AFM) and small angle x-ray scattering in transmission (SAXS) and grazing-incidence (GISAXS) modes enabled to study

the material evolution from solution processing through to the manifestation of the mesoporous inorganic film after BCP removal. In-depth SE/EP analysis evidenced an increase of over 40% in mesopore diameter with HP swelling and a consistent scaling of the overall void volume and number of pores. Importantly, our analytical tool-box enabled us to study the effect of swelling on the connecting necks between adjacent pores, with observed increases as high as ≈35%, knowledge of which is crucial to sensing, electrochemical and other mass transfer-dependent applications.

**Keywords:** block copolymers; structure directing agent; co-assembly; mesoporous films; pore swelling; micelles; ellipsometric porosimetry

# Introduction

Mesoporous inorganic film architectures are important components in applications such as photovoltaics,[1] protective optical coatings,[2,3] nanophotonics,[4] superconductors[5] and varied sensing applications.[6–8] A number of bottom-up self assembly methods offer control over the mesoscale material arrangement, including colloidal self-assembly,[9] polymeric porogens,[8,10] and sacrificial "structure-directing agents" (SDAs) such as small molecule surfactants[11,12] or block copolymers (BCPs)[13–15] These SDAs interact with inorganic precursors (typically sol-gel derived) in solution and produce ordered hybrid films via evaporation induced co-assembly before being removed to reveal the porous network.[16,17]

Pore size is a often a crucial parameter for material function, as demonstrated for mesoporous sensors,[6,18,19] photocatalytic materials,[20] perovskite and dye-sensitized solar cells,[1,21] humidity regulation[22] and catalysis.[23] In co-assembly, the size of the pore-forming block directly impacts the length scale of material arrangement. Pore sizes as low as 2 nm were accessed using small molecule surfactants[24] while the synthesis of block copolymers with larger molecular weight enabled to achieve pore sizes greater than 50 nm.[2,25]

For BCP co-assembly, the resultant pore size of the mesoporous film was shown to agree closely with scaling laws for the radius of gyration of the pore forming segment of the

BCP.[2,26–28] Nevertheless, pore size control via bespoke BCP synthesis can be a lengthy process. Consequently, alternative methods of pore size tuning have been investigated in both bulk and thin film materials.

A variety of small molecule "swelling agents" were utilised to increase the micelle core size and subsequent pore diameter, typically for silica bulk materials co-assembled by pluronic (poly(ethylene oxide)-*block*-poly(propylene oxide)-*block*-poly(ethylene oxide)).[29] The swelling agents were selected for their compatibility with the core forming block of the micelle, with examples including toluene,[30,31] xylene and ethylbenzene[30] as well as bulkier benzene derivatives.[32–35] It is important to note that these swelling techniques often required close control of reaction conditions, in particular the synthesis temperature.[30,31,35]

In purely organic assemblies, homopolymers (HPs), identical or chemically-similar to one of the BCP blocks, have shown capability to swell the core of micelles.[36–41] The swelling-induced increase in the micelle core dimeter was found to be related to the relative molecular weight $\mu$ and the volume fraction $\phi$ of the HP in relation to its BCP analogue, the compatibility of the solvent for the HP, the degree of chemical incompatibility of the HP and corona forming BCP block ($\chi_{\mathrm{HP,A;BCP,B}}$) and the incompatibility of the two BCP blocks($\chi_{\mathrm{A,B}}$).[36–41] Transitions in the micelle morphology as well as macroscopic phase separation have been observed upon increases of $\mu$ and $\phi$ beyond a critical limit.[36,38,40,42,43] This concept has been successfully implemented for pore expansion in bulk materials co-assembly.[44–46]

The implementation of pore expansion strategies for the co-assembly of mesoporous thin films has been subject of numerous studies.[47–52] Multiple challenges exist in a film materials architecture. Smaller, more volatile pore swelling agents are susceptible to evaporation during the evaporation induced co-assembly process while macroscopic phase separation of HP and BCP components have been reported.[47,49,50] Other issues include the onset of multimodal porosity, a significant increase in pore size distributions[47,49–51] and decreased long-range order with increased amount of homopolymer swelling agent.[50] Recently, Stefik and coworkers presented access to a greatly increased range of pore expansion by homopolymer swelling

based on the kinetic control offered by so-called persistent micelle templates.[52]

In this work, we use the amphiphilic block copolymer poly(isobutylene)-*block*-poly(ethylene oxide) (PIB-*b*-PEO) combined with poly(isobutylene) (PIB) homopolymer ($PIB_{HP}$) as a pore swelling agent for the co-assembly of mesoporous aluminosilicate films. PIB-*b*-PEO is an excellent candidate for structure directing applications due to the high chemical incompatibility of the two blocks and tendency to form well defined and stable micellar assemblies from a range of different block sizes.[53–58] We demonstrate a comprehensive structural characterisation suite with spectroscopic ellipsometry (SE) and ellipsometric porosimetry (EP) supplementing the more widely used atomic force microscopy (AFM), as well as small angle x-ray scattering in transmission (SAXS) and grazing incidence (GISAXS) modes. Importantly, EP and GISAXS provide the advantage of being able to probe the pore arrangement throughout the film, thus offering a more representative picture in comparison to surface based imaging techniques. This multifaceted analysis allows us to investigate the effect of homopolymer swelling at various processing stages, from micelle formation to hybrid film assembly and subsequent development into a mesoporous inorganic film architecture and relate findings on the resulting mesoporous networks to the underlying micelle co-assembly.

# Experimental

## Mesoporous aluminosilicate thin film preparation

$PIB_{39}$-*b*-$PEO_{36}$ BCP ($M_n$ 4.85 kg/mol; polydispersity index 1.26) was supplied by BASF following a previously reported synthetic route.[55] Inorganic sol material was synthesized as described elsewhere.[3,17] PIB HPs were purchased from Polymer Source in two different molecular weights, referred to as PIB800 ($M_n$ 0.8 kg/mol; polydispersity index 1.22) and PIB1500 ($M_n$ 1.5 kg/mol; polydispersity index 1.20). All polymer samples were first dissolved in toluene/1-butanol azeotrope solution then filtered using 0.2 $\mu$L syringe filter before mixing in desired ratios. All samples were prepared as described in table 1.

Table 1: List of materials and samples prepared during this work.

| Sample name | Mass of BCP (mg) | Mass of HP (mg) | Mass of sol (mg) | Volume of azeotrope (ml) |
|---|---|---|---|---|
| $BCP_{ref}$ | 5 | 0 | 40 | 0.238 |
| $BCP/PIB_{0.3}$ | 5 | 0.7 | 40 | 0.238 |
| $BCP/PIB_{0.5}$ | 5 | 1.2 | 40 | 0.238 |
| $BCP/PIB_{0.8}$ | 5 | 1.9 | 40 | 0.238 |

Mesoporous inorganic aluminosilicate films were prepared as described elsewhere.[3,17] For samples containing $PIB_{HP}$, the nomenclature $BCP/PIB(MW)_{\phi}$ indicates the mixture of BCP and $PIB_{HP}$. For example, $BCP/PIB(800)_{0.3}$ refers to a sample with PIB homopolymer of Mn 0.8 kg/mol at a volume ratio $PIB_{HP}$ / $PIB_{BCP}$ of $\phi = 0.3$. Before addition of aluminosilicate sol, hybrid BCP/HP mixtures were agitated for 1 hour on a rotary shaker at 500 rpm followed by addition of inorganic sol and further shaking for 1 hour using the same settings. All samples were spin-coated at 2000 rpm for 20 seconds and immediately annealed on a programmable hot plate using a ramp rate of 1 °C per min to a final temperature of 130 °C for 30 minutes. To remove the organic SDA, samples were calcined in a muffle furnace at 450 °C for 1 hour.

## Material Characterization

A Semilab SE2000 spectroscopic ellipsometer was used to perform spectroscopic ellipsometry (SE) and water-based environmental ellipsometric porosimetry (EP) measurements. All SE and EP data analysis was performed on the Semilabs SEA software (v1.6.2). Toluene-based EP measurements were performed using a Semilab PS2000 ellipsometer. Prior to EP measurements, samples were placed on a hotplate at 120 °C for 10 minutes. This was to ensure that no residual atmospheric water molecules remained in the pores prior to measurement. EP porosity isotherms were derived from the evolution of the refractive index value as a function of relative humidity in the sample chamber.[59] Application of the Lorentz-Lorentz effective medium approximation allowed accurate determination of the overall porosity of each sample based on the change in refractive index as a consequence of capillary conden-

sation inside the mesopores.[3] The incremental onset of capillary condensation was related to the pore diameter of the material via the Kelvin Equation.[59,60] Pore size and pore volume measurements were derived from the adsorption branches of the EP porosity isotherm and adjusted based on the assumption of an ellipsoidal pore shape which evolves with film contraction during template removal.[59] Pore neck measurements were determined from the desorption branch of the water-based EP isotherm. All pore sizes were further adjusted to account for the microscopic contact angle of $\approx 21\,^{\circ}$, which was calculated by comparing pore sizes obtained from EP using toluene (which wets the surface completely) and water (which exhibits a macroscopic contact angle) as sorbents.[61]

Liquid SAXS and GISAXS data were obtained on a SAXSLab Ganesha with GISAXS data acquired at an incidence angle of $0.2\,^{\circ}$. SAXS and GISAXS data analysis was performed using a combination of SAXSGUI (v2.23.16) and FitGISAXS..[62] Atomic Force Microscopy (AFM) images were obtained from a Bruker Dimension Icon atomic force microscope with a Bruker ScanAsyst Air probe (nominal tip radius 2 nm) in ScanAsyst mode.

## Results and discussion

The effect of HP swelling on the mesoporous architecture of aluminosilicate films was analysed using a combinatorial approach consisting of spectroscopic ellipsometry (SE) and ellipsometric porosimetry (EP) for pore size analysis with grazing-incidence small angle X-ray scattering (GISAXS) and atomic force microscopy (AFM) for structural characterisation.

Based on published studies of micellar systems in solution, it was expected that increasing a) the concentration of $PIB_{HP}$ relative to $PIB_{BCP}$ ($\phi$) and b) the MW of the $PIB_{HP}$ within the micelle would, in turn, influence the final pore diameter.[36–41] Liquid SAXS analysis of $BCP_{ref}$ and BCP/$PIB1500_{0.8}$ samples (Figure S1, Supplementary Information) confirmed the presence of spherical micelles in solution, which increased in size upon introduction of the HP swelling agent.[63] EP measurements were used to correlate the observed trends

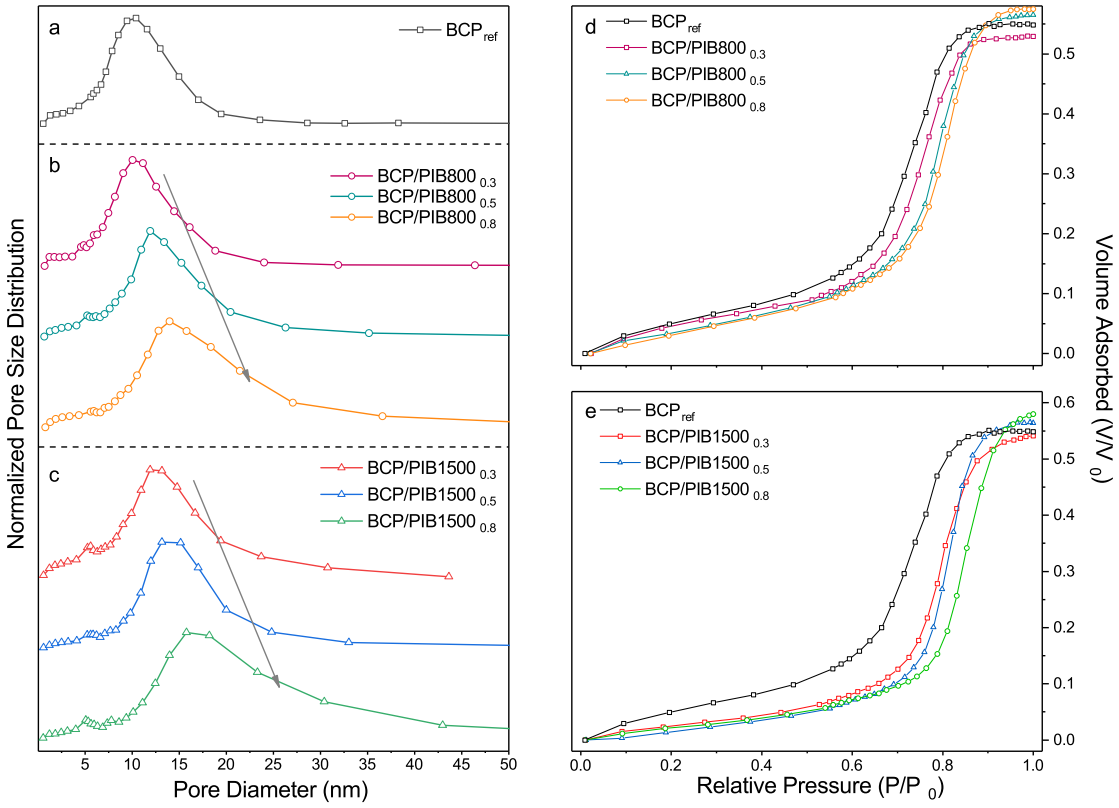


Figure 1: EP data for all samples. (a-c) Pore size distribution for (a) reference samples without HP swelling, (b) samples prepared with PIB800 HP and (c) samples prepared with PIB1500 HP. (d,e) EP adsorption isotherms for all samples.

for swelling BCP micelles in solution to the actual pore expansion in mesoporous films. Pore size distribution (PSD) data derived from EP measurements is displayed in Figure 1a-c. Pore diameter measurements obtained from EP were adjusted based on an expected ellipsoidal pore geometry, arising from film contraction due to BCP template removal.[59] The average film shrinkage was measured as ≈ 62 % in non-HP and ≈59 % in HP-swollen samples, indicating that the presence of HP had little effect on film contraction.

Almost all of BCP/PIB800 and BCP/PIB1500 samples exhibited notable increases in the pore diameter compared to $BCP_{ref}$ which measured a pore diameter of 10.1 (±0.8) nm. While the $BCP/PIB800_{0.3}$ sample exhibited little change in pore size with 10.3 (±0.6) nm, ratios of 0.5 and 0.8 displayed enlarged pore diameters of 11.6 (±0.6) nm and 13.9 (±0.8) nm respectively, providing rises of ≈14% and ≈36% when compared to $BCP_{ref}$. For BCP/PIB1500,

pore size increases were observed at all values of $\phi$.[64–66]

At each value of $\phi$, BCP/HP1500 samples exhibited greater expansion in pore size compared to similar $\phi$ values in the BCP/PIB800 samples. Pore diameters of 11.5 ($\pm$0.6) nm, 14.1 ($\pm$0.9) nm and 14.8 ($\pm$1.0) nm were measured at $\phi$ values of 0.3, 0.5 and 0.8 respectively. The pore size enlargement of $\approx$13%, $\approx$38% and $\approx$44% demonstrates that the higher MW of the swelling agent had a greater influence on resultant pore size at lower HP content when compared to BCP/PIB800. These findings are in line with earlier work, relating the formation of segregated domains within the micelle core to the higher penalty of mixing for larger MW polymers.[64–66] It should be noted that increasing $\phi$ to 1 resulted in visible deterioration of the film quality indicating that macroscopic phase separation of the $PIB_{HP}$ may have taken place. This echoes observations from previous studies of similar micellar systems.[36,38,67]

## Calculation of individual and overall pore volume

Table 2: Pore and void volume data calculated from SE and EP measurements

| Sample name | Pore diameter (nm) | Individual pore volume ($cm^3$)(*$10^{-19}$) | Number of pores (*$10^{13}$) | Total void volume ($cm^3$)(*$10^{-6}$) |
|---|---|---|---|---|
| $BCP_{ref}$ | 10.2 ± 0.7 | 1.8±0.2 | 4.1 ± 0.7 | 7.1±0.4 |
| $BCP/PIB800_{0.3}$ | 10.4 ± 0.5 | 1.9±0.3 | 3.5 ± 0.5 | 6.2±0.3 |
| $BCP/PIB800_{0.5}$ | 11.6 ± 0.6 | 2.6±0.4 | 2.7 ± 0.3 | 7.0±0.6 |
| $BCP/PIB800_{0.8}$ | 13.9 ± 0.8 | 4.4±0.7 | 1.8 ± 0.3 | 7.7±0.5 |
| $BCP/PIB1500_{0.3}$ | 11.5 ± 0.6 | 2.5±0.4 | 2.5 ± 0.3 | 6.5±0.7 |
| $BCP/PIB1500_{0.5}$ | 14.1 ± 0.9 | 4.6±0.9 | 1.7 ± 0.3 | 7.4±0.5 |
| $BCP/PIB1500_{0.8}$ | 14.8 ± 1.0 | 5.3±1.1 | 1.7 ± 0.3 | 8.5±0.6 |

Alongside expanded pore sizes were expected with increasing HP content, concurrent rises in sample porosity and film thickness were also observed with higher contents of HP (Figure 1d,e & Table S1, Supplementary Information) It is well established that, when preparing mesoporous films from BCP SDAs, the sample porosity is directly related to the BCP to inorganic ratio.[2,3] While all samples were prepared with a constant BCP to inorganic ratio (Table 1), the porosity increased from $\approx$50% in $BCP_{ref}$ to as high as $\approx$60% in $BCP/PIB1500_{0.8}$ as a consequence of the HP addition. Similarly, thickness values were found to gradually rise in BCP/HP samples with higher HP content. While increases in material

porosity derived from micelle swelling were reported before,[47,68] here, using a combination of SE and EP, we can provide a rationale for these trends. Combining film thickness and porosity data, the overall void volume was calculated per unit area (here 1 $cm^2$) of the film while the number of pores within the same volume was estimated by calculating the volume of each ellipsoidal pore[59] and dividing the total void volume by this value (Table 2). From this analysis a clear trend emerged: with increasing HP content, the individual pore volume and overall void volume within the film increased while the estimated number of pores decreased. The overall void volume for HP swollen samples shows a linear trend with $\phi$ for both BCP/PIB800 and BCP/PIB1500 samples (Figure S2a, Supplementary Information). A similar linear trend was observed in relation to the number of pores in BCP/PIB800 samples (Figure S2b, Supplementary Information). However, for BCP/PIB1500, the number of pores exhibited a plateau between $0.5 < \phi < 0.8$. This may be attributed to the fact that a maximum amount of PIB1500 was incorporated into the micelle core before macroscopic phase separation took place.[41]

These results provide a clear indication that the presence of HP had an effect, not only on the size of the micelle core in the hybrid solution, but also on the aggregation number of each micelle and the total number of micelles. The trend for higher aggregation numbers and reduction in overall number of micelles is consistent with previous reports on solution-based studies.[36,69–71] From a free energy perspective, when molecules are solubilized within the micelle core, increases to the aggregation number of the micelle reduce the overall free energy of the micellar system by minimizing both the free energy of dilution of the core-forming block and the interfacial free energy between the micelle core and the solvent.[70] Larger micelle core volumes are required in order to accommodate the bigger HP,[71] which is consistent with our findings of higher void volumes for BCP/PIB1500 when compared to BCP/PIB800 (Table 2). Here, using SE and EP analysis, we can confirm that the effect of HP swelling on individual micelles in solution also extends to porous inorganic materials derived from sacrificial BCP micelles following coating and template removal.

Note that, if required, the increase in film porosity with increasing HP content can be mitigated due to the flexibility of the BCP co-assembly approach. For BCP/PIB1500$_{0.8}$, pore sizes were maintained at ≈14.5 nm while porosity was reduced to ≈50% by simply reducing the BCP to inorganic ratio in the hybrid initial solution. (Figure S3, Supplementary Information).

While it is clear that the increased HP content results in enlarged pore diameter and pore volume within the film, it is also crucial to characterise the effects of HP swelling on the structure and order of the mesoporous material.

Analysis of EP isotherms can provide insightful information on the nature of the porous material being probed. All EP adsorption isotherms (Figure 1d,e) were classified as type IV curves as expected from mesoporous type materials.[72] The shape of the isotherm exhibited little change with increasing HP content indicating that the mesoporous nature of the porous network remains unchanged. No bimodal porosity was observed even at the highest loading of HP.

The EP adsorption/desorption isotherms provide a greater depth of information on the mesoporous structure throughout the film. Figure S4 (Supplementary Information) shows the adsorption/desorption isotherms for BCP$_{\text{ref}}$ (Figure S4a) and BCP/PIB1500$_{0.8}$ (Figure S4b). Both samples exhibited hysteresis loops between the adsorption and desorption branches. As per IUPAC, these hysteresis loops could potentially be classified as either H1 or H2.[73] Analysis based on the obtained hysteresis loop revealed an adsorption pore radius double in size of the desorption pore radius.[61,73] This would imply that, either pores were either cylindrical in shape (type H1) and the hysteresis took place due to the delayed condensation in the adsorption branch, or, that the pores were arranged in interconnected "ink-bottle" type networks (type H2), where the neck size distribution was of a similar scale to the main pore size distribution.[73]

To further evaluate these observations, EP measurements were performed on BCP$_{\text{ref}}$ using toluene as sorbent and the shape of the isotherm was compared to water-based EP (Figure

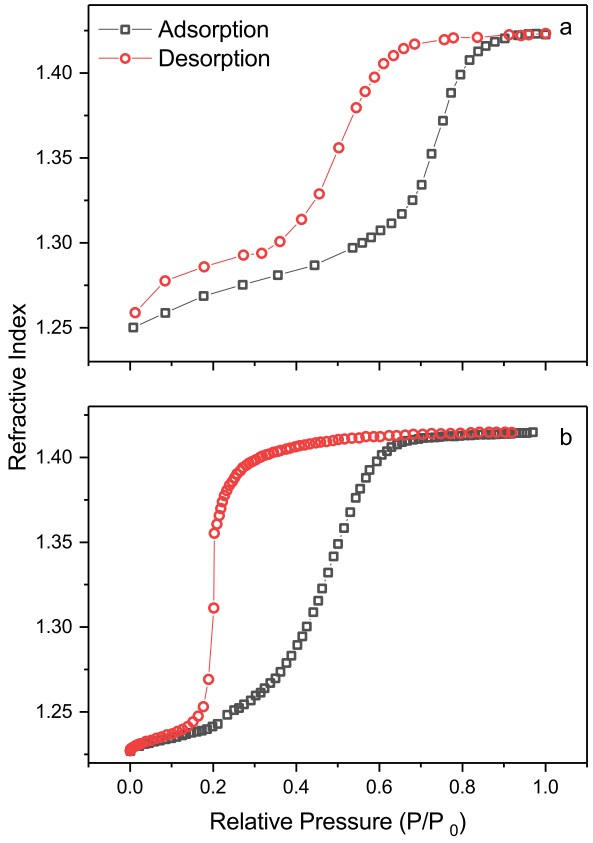


Figure 2: EP adsorption/desorption isotherms for $BCP_{ref}$. (a) Using water as sorbent. (b) Using toluene as sorbent

2). Where the water vapour EP (Figure 2a) exhibited a symmetric hysteresis loop, the toluene isotherm (Figure 2b) was asymmetric with a characteristic H2(a) hysteresis shape, which could only be attributed to narrow ink-bottle type interconnections, with evaporation being delayed due to the presence of interconnections that are narrower in size than the main pores.[74] The sudden onset of desorption at $P/P_0$ of $\approx 0.2$ was likely due to the phenomenon of cavitation, where the spontaneous nucleation of gas bubbles within the narrow restrictions causes the immediate evaporation of all liquid within the pores.[61,73] Toluene cavitation was reported at values of $P/P_0$ of $\approx 0.2$ in physisorption analysis of bulk powders[75] and observed in thin films using EP.[76] Due to cavitation taking place in the desorption branch of the toluene isotherm, no reliable quantitative data can be extracted from toluene-based EP in relation to the size of the pore neck.

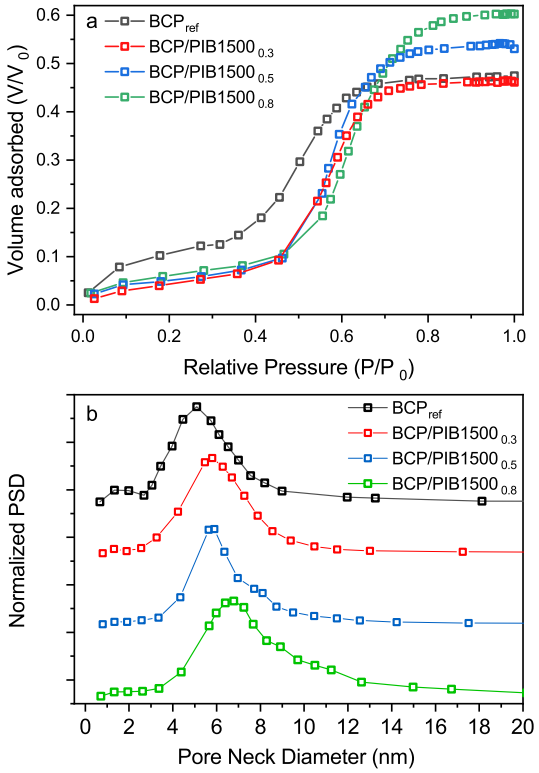


Figure 3: (a) EP desorption isotherms and (b) pore neck diameters obtained for $BCP_{ref}$ and BCP/PIB1500.

Given that cavitation effects were not observed during the water-based EP however, the desorption isotherms can be studied to investigate the impact of pore swelling on the size of these restrictions (Figure 3).[74] During desorption, the relative pressure at which the liquid water evaporates from the porous network (Figure 3a) provides information on the size of necks connecting the pores (Figure 3b), thus offering critically important information on the accessibility of pores throughout the network. Figure 3b shows that $BCP_{ref}$ exhibited pore openings of ≈5.2 nm which were expanded to sizes as high as ≈7 nm for BCP/PIB1500$_{0.8}$, representing an increase of ≈35%. Variations in the pore neck size have been reported when changing the nature of the SDA,[77] but here we demonstrate that it is possible to swell both the pore volume and pore interconnections using a swelling agent. It has been shown that the size of pore interconnections can have a direct impact on the liquid and vapour infiltration within the porous network[78,79] In more general terms, mass transport of molecules through

porous films is strongly dependent on open pores which are highly interconnected allowing for efficient diffusion of molecules through the network.[80] Such applications include electrochemistry,[81] nanoparticle synthesis,[77] sensing,[77,79] controlled release[82] and photocatalysis.[83] Successful use in application often relies on producing well defined films of target thickness without stress-induced cracking. Films of $\approx 120$ -$\dot{1}40$ nm were prepared during this work; this thickness range could be widened by increasing the concentration of material in the initial solution (up to hundreds of nm) and also combining with a proven layer-by-layer deposition technique (up to µm).[84] Furthermore, the BCP coassembly process is compatible with scalable liquid deposition and subsequent processing techniques.[17,85]

GISAXS (Figure 4) was carried out to analyse the in-plane structural characteristics of each sample in order to ensure that the ordering of the material was maintained even at higher loadings of HP swelling agent. 1-dimensional linecuts (Figure4) were performed along the $q_y$ axis of the 2D GISAXS scattering patterns (Figure 4, inset) to obtain information on the in-plane ordering. Each sample produced an in-plane scattering pattern that, upon data fitting, represented a hexagonal array of spherical objects.[62] This matched with similar patterns observed for non-swollen samples (Figure S5, Supplementary Information). In-plane *d*-spacing values provided information on the size of the repeating structural feature, in this instance, the centre to centre distance between pores. Consistent with the pore diameter measurements, incremental increases in *d*-spacing values were observed when compared to non-swollen counterparts providing further confirmation of the effects of HP swelling on the porous network. Measurements of the full-width at half-maximum (FWHM) of each 1-d linecut provided an indication of the extent of the order of each sample. Analysis of the primary scattering peak (Figure S7, Supplementary Information) showed minimal change in FWHM with incorporation of HP, suggesting a similar correlation length for pore ordering in all samples.

Combining GISAXS and pore size data enabled an estimation of the effects of HP pore swelling on the inter-pore wall thickness (Table S2, Supplementary Information). The pore

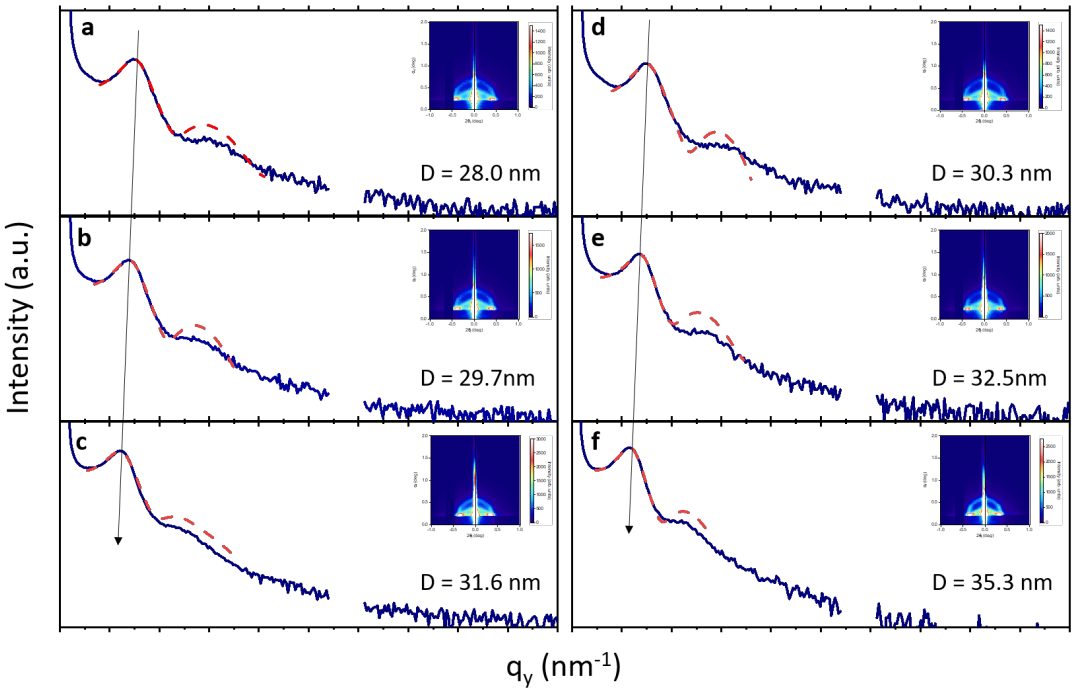


Figure 4: In-plane GISAXS linecuts along $q_y$ for HP swollen samples before BCP removal. (a-c) BCP/PIB800$_{0.3}$, BCP/PIB800$_{0.5}$ and BCP/PIB800$_{0.8}$ (d-f) BCP/PIB1500$_{0.3}$, BCP/PIB1500$_{0.5}$ and BCP/PIB1500$_{0.8}$. The dashed lines represent fitting patterns for spherical objects arranged in a 2D hexagonal paracrystalline array. 2D scattering patterns inset.

wall thickness data indicates a trend towards increased pore wall thickness as a function of HP loading. This can be expected when considering the trend towards increased pore volume and decreased number of pores calculated in Table 2.

AFM images (Figure 5, Figure S8 Supporting Information) provide visual confirmation of the presence of an ordered inverse opal type network on the surface of the material for all samples. This correlates with previously reported results using similar materials.[2,3,17] Fast Fourier transform (FFT) and correlation function of AFM images (Figure S6, Supplementary Information) of BCP$_{\text{ref}}$ and BCP/PIB1500$_{0.8}$ confirmed a similar extent of ordering in swollen and non-swollen samples, further demonstrating the capabilities of the herein presented approach.

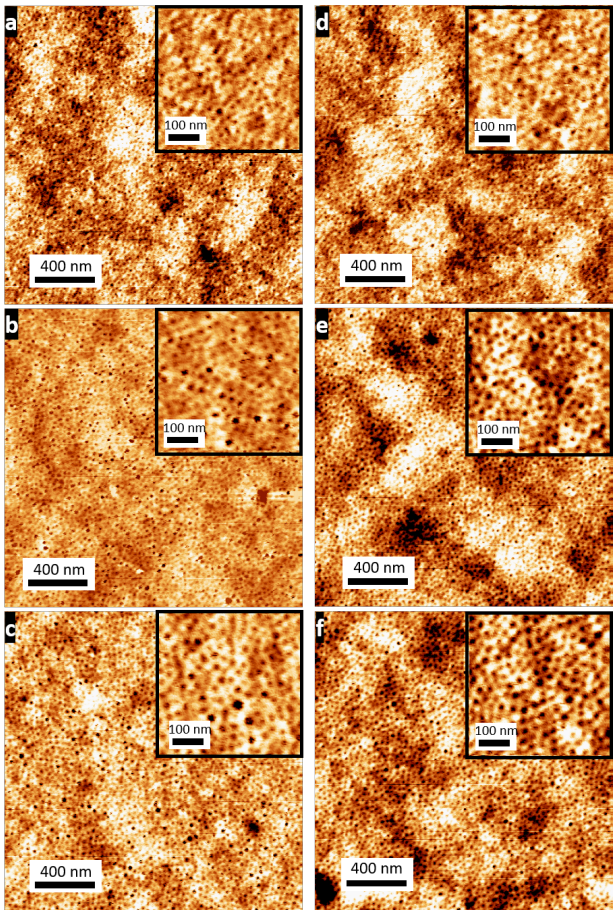


Figure 5: AFM images of all HP swollen samples. (a) BCP/PIB800$_{0.3}$, (b)BCP/PIB800$_{0.5}$, (c)BCP/PIB800$_{0.8}$, (d) BCP/PIB1500$_{0.3}$, (e)BCP/PIB1500$_{0.5}$, (f)BCP/PIB1500$_{0.8}$.

# Conclusions

In conclusion, we report pore size tuning in mesoporous aluminosilicate films using homopolymers (HPs) to swell the core of block copolymer (BCP) micelles in solution. A multifaceted analysis combining spectroscopic ellipsometry and ellipsometric porosimetry with SAXS, GISAXS and AFM enabled a unique insight into the effects of the swelling of micelles by HPs in solution on the resulting mesoporous network after film processing and removal of the structure-directing agent. Variation of both the molecular weight and volume fraction of the HP relative to the core forming block in the BCP enabled increases of over 40% to the pore size while simultaneously expanding the pore interconnections by up to 60%. Tuning of pore diameter and pore interconnections enables facile and bespoke adaption of

pore characteristics to the target application, with benefits envisioned for any mass transfer dependent application, ranging from electrochemistry and photocatalysis to sensing and controlled release.

## Acknowledgement

BR acknowledges funding by an EPSRC Industrial Case Award (EP/M506448/1) in support of BASF SE. SG and AAF are grateful for support by an EPSRC New Investigator Award (EP/R035105/1). The authors express gratitude to Dr Han Wu and the EPSRC CNIE research facility service (EPSRC Award, EP/K038656/1) at University College London for the collection of GISAXS data. The authors acknowledge Dr Peter Basa and Dr Bálint Fodor from Semilab (Budapest, Hungary) for performing EP measurements with toluene as sorbent. BR wishes to thank Salma Conway for preparation of schematic images.

## Supporting Information Available

Transmission SAXS measurements of hybrid micelles in solution; Pore and void volume data calculated from SE and EP measurements; Changes in pore volume and number of pores as a function of HP content; EP measurements for BCP/PIB1500$_{0.8}$ with lower BCP to inorganic ratio; EP adsorption/desorption isotherms for BCP$_{\text{ref}}$ and BCP/PIB1500$_{0.8}$; In-plane GISAXS linecuts along $q_y$ for unswollen BCP$_{\text{ref}}$ before template removal; Scanning electron microscope images of BCP$_{\text{ref}}$ and BCP/PIB1500$_{0.8}$; Full-width at half maximum measurements for fitted GISAXS peaks along along $q_y$ for all BCP$_{\text{ref}}$ and BCP/HP samples; Calculation of pore wall thickness from EP and GISAXS measurements; AFM image of BCP$_{\text{ref}}$

# References


(1) Shao, J.; Yang, S.; Lei, L.; Cao, Q.; Yu, Y.; Liu, Y. Pore Size Dependent Hysteresis Elimination in Perovskite Solar Cells Based on Highly Porous $TiO_2$ Films with Widely Tunable Pores of 15-34 nm. *Chem. Mater.* **2016**, *28*, 7134–7144.

(2) Guldin, S.; Kohn, P.; Stefik, M.; Song, J.; Divitini, G.; Ecarla, F.; Ducati, C.; Wiesner, U.; Steiner, U. Self-Cleaning Antireflective Optical Coatings. *Nano Lett.* **2013**, *13*, 5329–5335.

(3) Reid, B.; Taylor, A.; Chen, Y.; Schmidt-Hansberg, B.; Guldin, S. Robust Operation of Mesoporous Antireflective Coatings under Variable Ambient Conditions. *ACS Appl. Mater. Interfaces* **2018**, *10*, 10315–10321.

(4) Stefik, M.; Guldin, S.; Vignolini, S.; Wiesner, U.; Steiner, U. Block Copolymer Self-Assembly for Nanophotonics. *Chem. Soc. Rev.* **2015**, *44*, 5076–5091.

(5) Robbins, S. W.; Beaucage, P. A.; Sai, H.; Tan, K. W.; Werner, J. G.; Sethna, J. P.; DiSalvo, F. J.; Gruner, S. M.; Van Dover, R. B.; Wiesner, U. Block Copolymer Self-Assembly-Directed Synthesis of Mesoporous Gyroidal Superconductors. *Sci. Adv.* **2016**, *2*.

(6) Bearzotti, A.; Bertolo, J. M.; Innocenzi, P.; Falcaro, P.; Traversa, E. Humidity Sensors Based on Mesoporous Silica Thin Films Synthesised by Block Copolymers. *J. Eur. Ceram. Soc.* **2004**, *24*, 1969–1972.

(7) Nicole, L.; Boissière, C.; Grosso, D.; Hesemann, P.; Moreau, J.; Sanchez, C. Advanced Selective Optical Sensors Based on Periodically Organized Mesoporous Hybrid Silica Thin Films. *Chem. Commun.* **2004**, *10*, 2312–2313.

(8) Li, C.; Colella, N. S.; Watkins, J. J. Low-Temperature Fabrication of Mesoporous Titanium Dioxide Thin Films with Tunable Refractive Indices for One-Dimensional

Photonic Crystals and Sensors on Rigid and Flexible Substrates. *ACS Appl. Mater. Interfaces* **2015**, *7*, 13180–13188.

(9) Vogel, N.; Retsch, M.; Fustin, C.-A.; del Campo, A.; Jonas, U. Advances in Colloidal Assembly: The Design of Structure and Hierarchy in Two and Three Dimensions. *Chem. Rev.* **2015**, *115*, 6265–6311.

(10) Wang, C.; Li, L.; Zheng, S. Synthesis and Characterization of Mesoporous Silica Monoliths with Polystyrene Homopolymers as Porogens. *RSC Adv.* **2016**, *6*, 105840–105853.

(11) Matheron, M.; Bourgeois, A.; Brunet-Bruneau, A.; Albouy, P. A.; Biteau, J.; Gacoin, T.; Boilot, J. P. Highly Ordered CTAB-Templated Organosilicate Films. *J. Mater. Chem.* **2005**, *15*, 4741–4745.

(12) Goethals, F.; Ciofi, I.; Madia, O.; Vanstreels, K.; Baklanov, M. R.; Detavernier, C.; Van Der Voort, P.; Van Driessche, I. Ultra-Low-k Cyclic Carbon-Bridged PMO Films with a High Chemical Resistance. *J. Mater. Chem.* **2012**, *22*, 8281–8286.

(13) Templin, M.; Franck, A.; DuChesne, A.; Leist, H.; Zhang, Y. M.; Ulrich, R.; Schadler, V.; Wiesner, U. Organically Modified Aluminosilicate Mesostructures from Block Copolymer Phases. *Science* **1997**, *278*, 1795–1798.

(14) Zhao, D.; Feng, J.; Huo, Q.; Melosh, N.; Fredrickson, G.; Chmelka, B.; Stucky, G. Triblock Copolymer Syntheses of Mesoporous Silica with Periodic 50 to 300 Angstrom Pores. *Science* **1998**, *279*, 548–552.

(15) Wei, J.; Sun, Z.; Luo, W.; Li, Y.; Elzatahry, A. A.; Al-Enizi, A. M.; Deng, Y.; Zhao, D. New Insight into the Synthesis of Large-Pore Ordered Mesoporous Materials. *J. Am. Chem. Soc.* **2017**, *139*, 1706–1713.

(16) Grosso, D.; Cagnol, F.; Soler-Illia, G. J. d. A. A.; Crepaldi, E. L.; Amenitsch, H.;

Brunet-Bruneau, A.; Bourgeois, A.; Sanchez, C. Fundamentals of Mesostructuring Through Evaporation-Induced Self-Assembly. *Adv. Funct. Mater.* **2004**, *14*, 309–322.

(17) Reid, B.; Taylor, A.; Alvarez Fernandez, A.; Ismael, M. H.; Sharma, S.; Schmidt-Hansberg, B.; Guldin, S. Photocatalytic Template Removal by Non-Ozone Generating UV Radiation for the Fabrication of Well Defined Mesoporous Inorganic Coatings. *ACS Appl. Mater. Interfaces* **2019**, *11*, 19308–19314.

(18) Teoh, L. G.; Hon, Y. M.; Shieh, J.; Lai, W. H.; Hon, M. H. Sensitivity Properties of a Novel $NO_2$ Gas Sensor Based on Mesoporous $WO_3$ Thin Film. *Sensors Actuators, B Chem.* **2003**, *96*, 219–225.

(19) Walcarius, A. Mesoporous Materials-Based Electrochemical Sensors. *Electroanalysis* **2015**, *27*, 1303–1340.

(20) Kim, W.; Choi, S. Y.; Jeon, Y. M.; Lee, S. K.; Kim, S. H. Highly Ordered, Hierarchically Porous $TiO_2$ Films via Combination of Two Self-Assembling Templates. *ACS Appl. Mater. Interfaces* **2014**, *6*, 11484–11492.

(21) Docampo, P.; Guldin, S.; Leijtens, T.; Noel, N. K.; Steiner, U.; Snaith, H. J. Lessons Learned: From Dye-Sensitized Solar Cells to All-Solid-State Hybrid Devices. *Adv. Mater.* **2014**, *26*, 4013–4030.

(22) Lan, H.; Jing, Z.; Li, J.; Miao, J.; Chen, Y. Influence of Pore Dimensions of Materials on Humidity Self-regulating Performances. *Mater. Lett.* **2017**, *204*, 23–26.

(23) Zubrzycki, R.; Ressler, T. Influence of Pore Size of SBA-15 on Activity and Selectivity of $H_3[PMo_{12}O_{40}]$ Supported on Tailored SBA-15. *Microporous Mesoporous Mater.* **2015**, *214*, 8–14.

(24) Kim, M. J.; Ryoo, R. Synthesis and Pore Size Control of Cubic Mesoporous Silica SBA-1. *Chem. Mater.* **1999**, *11*, 487–491.

(25) Lokupitiya, H. N.; Jones, A.; Reid, B.; Guldin, S.; Stefik, M. Ordered Mesoporous to Macroporous Oxides with Tunable Isomorphic Architectures: Solution Criteria for Persistent Micelle Templates. *Chem. Mater.* **2016**, *28*, 1653–1667.

(26) Noolandi, J.; Hong, K. M. Theory of Block Copolymer Micelles in Solution. *Macromolecules* **1983**, *16*, 1443–1448.

(27) Rubinstein, M.; Colby, R. *Polymer Physics*; Oxford University Press, 2003; p 440.

(28) Bloch, E.; Llewellyn, P. L.; Phan, T.; Bertin, D.; Hornebecq, V. On Defining a Simple Empirical Relationship to Predict the Pore Size of Mesoporous Silicas Prepared from PEO-*b*-PS Diblock Copolymers. *Chem. Mater.* **2009**, *21*, 48–55.

(29) Kruk, M. Access to Ultralarge-Pore Ordered Mesoporous Materials through Selection of Surfactant/Swelling-Agent Micellar Templates. *Acc. Chem. Res.* **2012**, *45*, 1678–1687.

(30) Li, Y.; Kruk, M. Single-Micelle-Templated Synthesis of Hollow Silica Nanospheres with Tunable Pore Structures. *RSC Adv.* **2015**, *5*, 69870–69877.

(31) Huang, L.; Kruk, M. Versatile Surfactant/Swelling-agent Template for Synthesis of Large-pore Ordered Mesoporous Silicas and Related Hollow Nanoparticles. *Chem. Mater.* **2015**, *27*, 679–689.

(32) Boissière, C.; Martines, M. A.; Tokumoto, M.; Larbot, A.; Prouzet, E. Mechanisms of Pore Size Control in MSU-X Mesoporous Silica. *Chem. Mater.* **2003**, *15*, 509–515.

(33) Fan, J.; Yu, C.; Lei, J.; Zhang, Q.; Li, T.; Tu, B.; Zhou, W.; Zhao, D. Low-Temperature Strategy to Synthesize Highly Ordered Mesoporous Silicas with Very Large Pores. *J. Am. Chem. Soc.* **2005**, *127*, 10794–10795.

(34) Ma, G.; Yan, X.; Li, Y.; Xiao, L.; Huang, Z.; Lu, Y.; Fan, J. Ordered Nanoporous Silica with Periodic 30-60 nm Pores as an Effective Support for Gold Nanoparticle Catalysts with Enhanced Lifetime. *J. Am. Chem. Soc.* **2010**, *132*, 9596–9597.

(35) Yi, J.; Kruk, M. Pluronic-P123-Templated Synthesis of Silica with Cubic $Ia3d$ Structure in the Presence of Micelle Swelling Agent. *Langmuir* **2015**, *31*, 7623–7632.

(36) Tuzar, Z.; Bahadur, P.; Kratochvil, P. Solubilization of Homopolymers and Co-Polymers by Block Co-Polymer Micelles in Dilute-Solutions. *Makromol. Chem.* **1981**, *182*, 1751–1760.

(37) Price, C.; Stubbersfield, R. Solubilisation of Homopolystyrenes by Micelles Formed by a Polystyrene-*b*-poly(ethylene/propylene) Copolymer in a Base Lubricating Oil. *Eur. Polym. J.* **1987**, *23*, 177–179.

(38) Quintana, J. R.; Salazar, R. A.; Katime, I. Solubilization of Polyisobutylene by Polystyrene-block-poly(ethylene/propylene) Micelles. *Macromolecules* **1994**, *27*, 665–668.

(39) Whitmore, M. D.; Smith, T. W. Swelling of Copolymer Micelles by Added Homopolymer. *Macromolecules* **1994**, *27*, 4673–4683.

(40) Prahsarn, C.; Jamieson, A. M. Morphological Studies of Binary Homopolymer/Block Copolymer Blends: Effect of Molecular Weight. *Polymer* **1997**, *38*, 1273–1283.

(41) Izzo, D.; Marques, C. M. Solubilization of Homopolymers in a Solution of Diblock Copolymers. *J. Phys. Chem. B* **2005**, *109*, 6140–6145.

(42) Winey, K. I.; Thomas, E. L.; Fetters, L. J. Isothermal Morphology Diagrams for Binary Blends of Diblock Copolymer and Homopolymer. *Macromolecules* **1992**, *25*, 2645–2650.

(43) Jeon, K. J.; Roe, R. J. Solubilization of a Homopolymer in a Block Copolymer. *Macromolecules* **1994**, *27*, 2439–2447.

(44) Park, B. G.; Guo, W.; Cui, X.; Park, J.; Ha, C. S. Preparation and Characterization of Organo-Modified SBA-15 by Using Polypropylene Glycol as a Swelling Agent. *Microporous Mesoporous Mater.* **2003**, *66*, 229–238.

(45) Deng, Y.; Liu, J.; Liu, C.; Gu, D.; Sun, Z.; Wei, J.; Zhang, J.; Zhang, L.; Tu, B.; Zhao, D. Ultra-Large-Pore Mesoporous Carbons Templated from Polyethylene oxide-*b*-polystyrene Diblock Copolymer by Adding Polystyrene Homopolymer as a Pore Expander. *Chem. Mater.* **2008**, *20*, 7281–7286.

(46) Wei, J.; Deng, Y.; Zhang, J.; Sun, Z.; Tu, B.; Zhao, D. Large-pore Ordered Mesoporous Carbons with Tunable Structures and Pore Sizes Templated from Poly(ethylene oxide)-*b*-poly(methyl methacrylate). *Solid State Sci.* **2011**, *13*, 784–792.

(47) Hwang, Y. K.; Patil, K. R.; Jhung, S. H.; Chang, J. S.; Ko, Y. J.; Park, S. E. Control of Pore Size and Condensation Rate of Cubic Mesoporous Silica Thin Films using a Swelling Agent. *Microporous Mesoporous Mater.* **2005**, *78*, 245–253.

(48) Perlich, J.; Schulz, L.; Abul Kashem, M. M.; Cheng, Y.-J.; Memesa, M.; Gutmann, J. S.; Roth, S. V.; Müller-Buschbaum, P. Modification of the Morphology of P(S-b-EO) Templated Thin $TiO_2$ Films by Swelling with PS Homopolymer. *Langmuir* **2007**, *23*, 10299–10306.

(49) Malfatti, L.; Bellino, M. G.; Innocenzi, P.; Soler-Illia, G. J. A. A. One-Pot Route to Produce Hierarchically Porous Titania Thin Films by Controlled Self-Assembly, swelling, and phase separation. *Chem. Mater.* **2009**, *21*, 2763–2769.

(50) Wu, Q. L.; Rankin, S. E. Tuning the Mesopore Size of Titania Thin Films using a Polymeric Swelling Agent. *J. Phys. Chem. C* **2011**, *115*, 11925–11933.

(51) Dunphy, D. R.; Sheth, P. H.; Garcia, F. L.; Brinker, C. J. Enlarged Pore Size in Mesoporous Silica Films Templated by Pluronic F127: Use of Poloxamer Mixtures and Increased Template/$SiO_2$ Ratios in Materials Synthesized by Evaporation-Induced Self-Assembly. *Chem. Mater.* **2015**, *27*, 75–84.

(52) Sarkar, A.; Thyagarajan, A.; Cole, A.; Stefik, M. Widely Tunable Persistent Micelle Templates via Homopolymer Swelling. *Soft Matter* **2019**,

(53) Groenewolt, M.; Brezesinski, T.; Schlaad, H.; Antonietti, M.; Groh, P. W.; Iván, B. Polyisobutylene-*block*-Poly(ethylene oxide) for Robust Templating of Highly Ordered Mesoporous Materials. *Adv. Mater.* **2005**, *17*, 1158–1162.

(54) Schulz, M.; Glatte, D.; Meister, A.; Scholtysek, P.; Kerth, A.; Blume, A.; Bacia, K.; Binder, W. H. Hybrid Lipid/Polymer Giant Unilamellar Vesicles: Effects of Incorporated Biocompatible PIB-PEO Block Copolymers on Vesicle Properties. *Soft Matter* **2011**, *7*, 8100.

(55) von Graberg, T.; Hartmann, P.; Rein, A.; Gross, S.; Seelandt, B.; Röger, C.; Zieba, R.; Traut, A.; Wark, M.; Janek, J.; Smarsly, B. M. Mesoporous Tin-Doped Indium Oxide Thin Films: Effect of Mesostructure on Electrical Conductivity. *Sci. Technol. Adv. Mater.* **2011**, *12*, 025005.

(56) Sallard, S.; Schröder, M.; Boissière, C.; Dunkel, C.; Etienne, M.; Walcarius, A.; Oekermann, T.; Wark, M.; Smarsly, B. M. Bimodal Mesoporous Titanium Dioxide Anatase Films Templated by a Block Polymer and an Ionic Liquid: Influence of the Porosity on the Permeability. *Nanoscale* **2013**, *5*, 12316–29.

(57) Weidmann, C.; Brezesinski, K.; Suchomski, C.; Tropp, K.; Grosser, N.; Haetge, J.; Smarsly, B. M.; Brezesinski, T. Morphology-Controlled Synthesis of Nanocrystalline $\eta$-$Al_2O_3$ Thin Films, Powders, Microbeads, and Nanofibers with Tunable Pore Sizes from Preformed Oligomeric Oxo-Hydroxo Building Blocks. *Chem. Mater.* **2012**, *24*, 486–494.

(58) Reitz, C.; Haetge, J.; Suchomski, C.; Brezesinski, T. Facile and General Synthesis of Thermally Stable Ordered Mesoporous Rare-Earth Oxide Ceramic Thin Films with Uniform Mid-Size to Large-Size Pores and Strong Crystalline Texture. *Chem. Mater.* **2013**, *25*, 4633–4642.

(59) Boissiere, C.; Grosso, D.; Lepoutre, S.; Nicole, L.; Bruneau, A. B.; Sanchez, C. Poros-

ity and Mechanical Properties of Mesoporous Thin Films Assessed by Environmental Ellipsometric Porosimetry. *Langmuir* **2005**, *21*, 12362–12371.

(60) Baklanov, M. R.; Mogilnikov, K. P.; Polovinkin, V. G.; Dultsev, F. N. Determination of Pore Size Distribution in Thin Films by Ellipsometric Porosimetry. *J. Vac. Sci. Technol. B Microelectron. Nanom. Struct.* **2000**, *18*, 1385.

(61) Baklanov, M.; Green, M.; Maex, K. *Dielectr. Film. Adv. Microelectron.*; John Wiley & Sons, Ltd: Chichester, UK, 2007; p 129.

(62) Babonneau, D. FitGISAXS : Software Package for Modelling and Analysis of GISAXS Data using IGOR Pro. *J. Appl. Crystallogr.* **2010**, *43*, 929–936.

(63) Kikhney, A. G.; Svergun, D. I. A Practical Guide to Small Angle X-ray Scattering (SAXS) of Flexible and Intrinsically Disordered Proteins. *FEBS Lett.* **2015**, *589*, 2570–7.

(64) Hashimoto, T.; Tanaka, H.; Hasegawa, H. Ordered Structure in Mixtures of a Block Copolymer and Homopolymers. 2. Effects of Molecular Weights of Homopolymers. *Macromolecules* **1990**, *23*, 4378–4386.

(65) Viduna, D.; Limpouchová, Z.; Procházka, K. Conformation of Chains in Cores of Block Copolymer Micelles with Solubilized Homopolymer: A Monte Carlo Study. *Macromol. Theory Simulations* **2001**, *10*, 165–173.

(66) Lefebvre, M. D.; Shull, K. R. Homopolymer Solubilization and Nanoparticle Encapsulation in Diblock Copolymer Micelles. *Macromolecules* **2006**, *39*, 3450–3457.

(67) Pépin, M. P.; Whitmore, M. D. Homopolymer Solubilization Limits in Copolymer Micelles: A Monte Carlo Study. *Macromolecules* **2000**, *33*, 8654–8662.

(68) Cao, L.; Man, T.; Kruk, M. Synthesis of Ultra-Large-Pore SBA-15 Silica with Two-Dimensional Hexagonal Structure using Triisopropylbenzene as Micelle Expander. *Chem. Mater.* **2009**, *21*, 1144–1153.

(69) Tuzar, Z.; Kratochvil, P. Block and Graft Copolymer Micelles in Solution. *Adv. Colloid Interface Sci.* **1976**, *6*, 201–232.

(70) Nagarajan, R.; Ganesh, K. Block copolymer self-assembly in selective solvents: theory of solubilization in spherical micelles. *Macromolecules* **1989**, *22*, 4312–4325.

(71) Quintana, J. R.; Salazar, R. A.; Katime, I. Solubilization of Homopolymers by Block Copolymer Micelles in Dilute Solutions: Laser Light Scattering and Viscosity Studies on Micellar Solutions. *J. Phys. Chem.* **1995**, *99*, 3723–3731.

(72) Sing, K. S. W. Reporting Physisorption Data for Gas/Solid Systems with Special Reference to the Determination of Surface Area and Porosity. *Pure Appl. Chem.* **1985**, *57*, 603–619.

(73) Thommes, M.; Kaneko, K.; Neimark, A. V.; Olivier, J. P.; Rodriguez-Reinoso, F.; Rouquerol, J.; Sing, K. S. W. Physisorption of Gases, with Special Reference to the Evaluation of Surface Area and Pore Size Distribution (IUPAC Technical Report). *Pure And Applied Chemistry* **2015**, *87*, 1051–1069.

(74) Thommes, M.; Cychosz, K. A. Physical Adsorption Characterization of Nanoporous Materials: Progress and challenges. *Adsorption* **2014**, *20*, 233–250.

(75) Ravikovitch, P. I.; Vishnyakov, A.; Neimark, A. V.; Ribeiro Carrott, M. M. L.; Russo, P. A.; Carrott, P. J. Characterization of Micro-Mesoporous Materials from Nitrogen and Toluene Adsorption: Experiment and Modeling. *Langmuir* **2006**, *22*, 513–516.

(76) Yim, J. H.; Seon, J. B.; Jeong, H. D.; Pu, L. S.; Baklanov, M. R.; Gidley, D. W. Morphological Control of Nanoporous Films by the Use of Functionalized Cyclodextrins as Porogens. *Adv. Funct. Mater.* **2004**, *14*, 277–282.

(77) Steinberg, P. Y.; Zalduendo, M. M.; Giménez, G.; Soler-Illia, G. J. A. A.; Angelomé, P. C. $TiO_2$ Mesoporous Thin Film Architecture as a Tool to Control Au Nanoparticles Growth and Sensing Capabilities. *Phys. Chem. Chem. Phys.* **2019**, *21*, 10347–10356.

(78) Ceratti, D. R.; Faustini, M.; Sinturel, C.; Vayer, M.; Dahirel, V.; Jardat, M.; Grosso, D. Critical effect of Pore Characteristics on Capillary Infiltration in Mesoporous Films. *Nanoscale* **2015**, *7*, 5371–5382.

(79) Angiolini, J. F.; Stortz, M.; Steinberg, P. Y.; Mocskos, E.; Bruno, L.; Soler-Illia, G.; Angelomé, P. C.; Wolosiuk, A.; Levi, V. Diffusion of Single Dye Molecules in Hydrated $TiO_2$ Mesoporous Films. *Phys. Chem. Chem. Phys.* **2017**, *19*, 26540–26544.

(80) Walcarius, A. Mesoporous Materials-Based Electrochemical Sensors. *Electroanalysis* **2015**, *27*, 1303–1340.

(81) Alberti, S.; Steinberg, P. Y.; Giménez, G.; Amenitsch, H.; Ybarra, G.; Azzaroni, O.; Angelomé, P. C.; Soler-Illia, G. J. Chemical Stability of Mesoporous Oxide Thin Film Electrodes under Electrochemical Cycling: From Dissolution to Stabilization. *Langmuir* **2019**, *35*, 6279–6287.

(82) Lian, H. Y.; Liang, Y. H.; Yamauchi, Y.; Wu, K. C.-W. A Hierarchical Study on Load/Release Kinetics of Guest Molecules into/from Mesoporous Silica Thin Films. *J. Phys. Chem. C* **2011**, *115*, 6581–6590.

(83) Carreon, M. A.; Choi, S. Y.; Mamak, M.; Chopra, N.; Ozin, G. A. Pore Architecture Affects Photocatalytic Activity of Periodic Mesoporous Nanocrystalline Anatase Thin Films. *J. Mater. Chem.* **2007**, *17*, 82–89.

(84) Guldin, S.; Docampo, P.; Stefik, M.; Kamita, G.; Wiesner, U.; Snaith, H. J.; Steiner, U. Layer-by-Layer Formation of Block-Copolymer-Derived $TiO_2$ for Solid-State Dye-Sensitized Solar Cells. *Small* **2012**, *8*, 432–440.

(85) Sanchez, C.; Belleville, P.; Popall, M.; Nicole, L. Applications of Advanced Hybrid Organic-Inorganic Nanomaterials: from Laboratory to Market. *Chem. Soc. Rev.* **2011**, *40*, 696.

# Graphical TOC Entry